Original Study

Open Access

Queen Arista Rosmania Putri Sumarsono*, As'ad Munawir, Harimurti

Comparative Analysis of Single Pile with Embedded Beam Row and Volume Pile Modeling under Seismic Load

https://doi.org/10.2478/sgem-2022-0027
received April 28, 2022; accepted October 23, 2022.

Abstract: Indonesia is located between the Eurasian, Pacific, Philippines, and Indo-Australian plates. Various tectonic processes in the world and collisions between large plates and several small plates trigger many earthquakes in Indonesia. This study aimed to evaluate the response of bored piles in the Auditorium Building of Brawijaya University toward seismic loads through analytical and numerical approaches based on finite elements with 2D (embedded beam row) and 3D (volume pile) modeling, where the analysis approach of pile deformation and lateral resistance with numerical methods will depend on idealization of the model used. In addition, the lateral resistance was compared based on combination lateral loads, pile stiffness, and soil stiffness when the values were different. The 2D finite element analysis reduces lateral resistance but overestimated the deflection on the pile surface. This is because in the 2D finite element modeling with an embedded beam row that the friction factor represented by the spring can reduces the stiffness and the pile–soil is tangent, so that there is no slipping against each other. In addition, the 3D finite element analysis with volume pile modeling increases soil stiffness at greater depths and the friction factor (interface) can improve the interaction between the soil and pile.

Keywords: finite element method; lateral pile; lateral resistance; seismic load.

***Corresponding author: Queen Arista Rosmania Putri Sumarsono,** Civil Engineering Department, Brawijaya University, Indonesia, E-mail: queenarps00@gmail.com
As'ad Munawir, Harimurti, Civil Engineering Department, Brawijaya University, Indonesia

1 Introduction

Earthquakes are natural phenomena that cannot be avoided or prevented. Indonesia is at high risk for earthquakes because of its location between the Eurasian, the Pacific, the Philippines, and the Indo-Australian plate. Predicting earthquakes accurately is challenging. Therefore, Indonesia is in danger posed by earthquakes. An earthquake of magnitude 6.1 in South Malang resulted in 10 deaths. Hundreds were injured, and it caused much damage to buildings. This earthquake was not the first earthquake in 2021. Several earthquakes have occurred, including a magnitude of 6.7 on November 20, 1958, based on the Meteorology Climatology Geophysics Agency in Karangkates Station, Indonesia. The earthquake caused minor damage to buildings with solid construction within VIII of Modified Mercalli Intensity.

Pile foundation behavior can be known through the response to load and deformation. The approach to analyzing pile deformation and lateral resistance with numerical methods depends on the idealization of the model. Sluis et al. [1] conducted the worst interaction performance of piles with embedded beam rows observed in the case of soil profiles with relatively rigid shallow soil layers. At Plaxis, these layers result in significant lateral earth pressure mobilization, exceeding the ultimate lateral soil capacity. In such cases, there is a redistribution of soil–structure interactions. Therefore, at high lateral pile loads under these soil conditions, caution should be exercised against unrealistic interaction behavior. For this study, a solution was found by iteratively adjusting the stiffness of the shallow soil group around the pile. Although this procedure is not ideal in terms of time, it is effective and allows designers to use piles with embedded beam rows as an excellent new feature of Plaxis 2D [1].

Three-dimensional Finite Element Modeling (3D-FEM) program is widely used to solve complex pile–soil interaction problems. Due to the three-dimensional nature and high degree of nonlinearity, the two-

dimensional finite element modeling of laterally loaded piles is fundamentally incorrect. Over time, many studies with 3D-FEM for laterally loaded single piles have been carried out. Brown et al. [2] modeled a single laterally loaded pile using a three-dimensional numerical finite element model. Another example of 3D-FEM is a study investigating the influence of pile and soil properties. The FEM model requires a considerable computational effort, which is not proposed for routine design, and is therefore not considered suitable for reliability updates [3].

Several studies were conducted to determine the response of the soil pile in the case of a single pile. Cao et al. [4] discuss in detail the effects of rotational soil flow and additional resistance components on the lateral soil-pillar behavior. Its validation was verified by centrifugal test and field test. The results showed that using the p–y API (American Petroleum Institute) method [5] reduces the ultimate lateral stiffness and resistance compared to the calculated results from 3D-FEA (Finite Element Analysis) [4].

Wang et al. [6] presented a numerical investigation to measure the effect of pile diameter and flexural stiffness on the load transfer curve (p–y curve) of a laterally loaded monopile in dense sand and to understand the primary mechanism governing diameter dependencies. The soil parameters for this calculation were from the Mustang Island soil test site. The results show that the API method [5] can provide reasonable predictions of up to 20%D deflection at the ground level for small-diameter piles. Initial rigors are well taken based on API methods. For further loading, it can be seen that the API method [5] reduces the bearing capacity of laterally loaded piles. The underestimation is less than 25% [6].

Comparing the pile models with numerical analysis with embedded beam rows and volumes is rarely done. Some studies only present research results using one of these models without further comparing the two. Therefore, this study evaluated the response of bored piles in the Auditorium Building of Universitas Brawijaya toward lateral loads, especially seismic loads, under equivalent static load conditions. Determining the pile should reduce the hazard of failure and collapse. This study was conducted using a single pile case and analyzed by analytical methods based on previous research, a numerical method based on 2D- and 3D-finite element methods. The output of this study is the distribution value of lateral resistance and the load-deflection response in the form of a p–y curve, with different cases in the values of combination lateral load, pile stiffness, and soil stiffness. The results should help to find out the behavioral of the single pile's foundation of the Auditorium Building, Brawijaya University, by embedded beam row and volume pile modeling, so that it can be seen the results of which analysis are best used in conditions that follow the field conditions. In addition, a comparison between numerical and analytical methods is necessary to obtain more accurate results.

2 Literature Review

2.1 Cyclic Load

Cyclic loading increases deflection and bending moment in short-term loading. Isenhower et al. [7] reported several studies with bored piles under cyclic lateral loading in overconsolidated clay soils without free water. The pile deflection at ground level is 25 mm during cyclic loading. After the load is removed, a gap appears in a pile (Figure 1). Thus, cracks are visible from the front [7].

Cyclic loading of piles in sandy soil in one direction will permanently deflect piles in the direction of loading. For example, a relatively sizable cyclic load is applied in one direction and the pile top will allow soil particles. Therefore, no cohesion is observed to fall into the open gaps at the back of the pile (Figure 1). Moreover, the pile cannot return to the original position after the cyclic loading and causes the development of permanent deflection [7].

2.2 p–y curve

The soil reaction to the pile (p) is related to the pile deflection (y) through a nonlinear load-deflection curve. The main drawback of the p–y method is the soil is not a continuum, but a series of discrete springs (i.e., the Winkler model). Winkler's approach is a good representation of the important pile–soil interaction in evaluating the response of pile to earthquake shaking. Winkler's approach to lateral pile analysis is widely used in practice because of its easy of nonlinear modeling and mathematical and computational efficiency.

Soil properties, pile geometry, and load properties are the most influential factors on the p–y curve. Soil properties are principally confined to the soil zone close to the pile friction, whereas soil masses of several pile diameters are pressured when lateral deflection occurs [8].

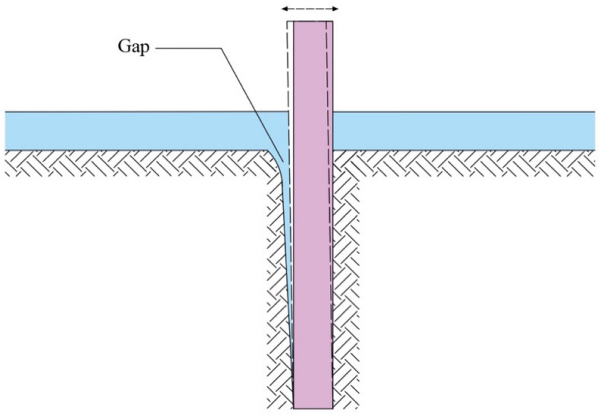

Figure 1: Pile due to cyclic load.

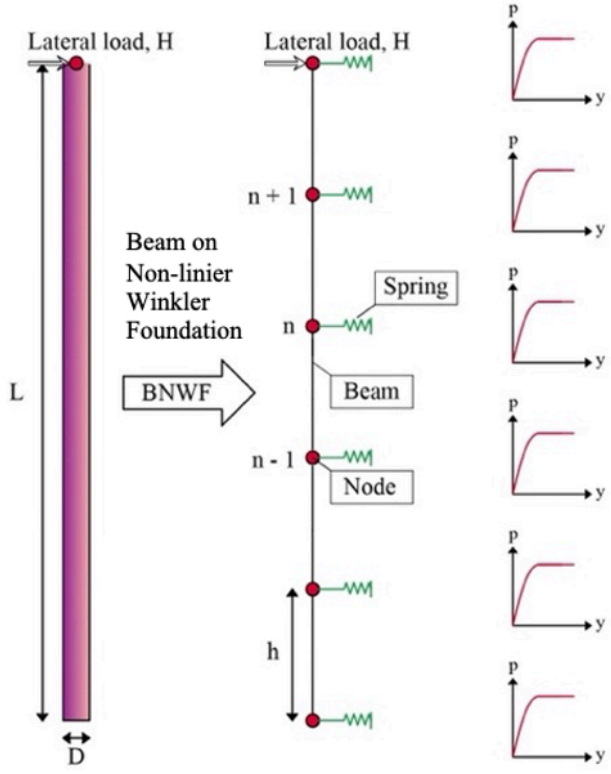

Figure 2: The p–y curve based on the Winkler's model.

2.2.1 API (2011)

The relationship of lateral deflection resistance (p–y) for sand is also nonlinear and can be estimated at a certain depth, H, by the following equation [9]:

$$p = Ap_u \times \tan h\left[\frac{k \times H}{A \times p_u} \times y\right] \quad (1)$$

where p = lateral soil strength per unit length of pile, y = pile deflection, A = factor under cyclic loading conditions = 0.90, p_u = lateral bearing capacity, k = subgrade reaction modulus, y = pile deflection, and H = depth.

Augustesen et al. (2009) in Wang et al. (2020) [6] propose the relationship of k with Equation (1) as follows:

$$k = (0.008085\varphi^{2.45} - 26.09) \times 10^3 \quad (2)$$

where φ = inner shear angle.

2.2.2 Klinkvort (2012)

Klinkvort (2012) conducted a series of centrifugal tests on pile diameters and proposed a new model for calculating nonlinear p–y curves. A hyperbolic formulation was adopted to redefine the shape of the p–y curve as follows [6]:

$$p = \frac{y}{\frac{1}{k_{ini}} + \frac{y}{Ap_u}} \quad (3)$$

where p = lateral soil strength per unit length of pile, y = pile deflection, p_u = lateral bearing capacity, and k_{ini} = initial stiffness. Assumed to be proportional to Rankine's passive earth pressure coefficient, $(K_p) = 100K_p \gamma z$, A = empirical depth correction coefficient = $0.9 + 1.1\left(\frac{1}{2} + \frac{1}{2}\tanh\left(9 - \frac{3z}{D}\right)\right)$

2.2.3 Liang et al. (2018)

A correction factor is used to modify the initial stiffness with the following equation to display the hyperbolic p–y curve closer to the shape of the API p–y curve [10]:

$$k_{ini} = \frac{\eta K^*.x}{5a \tanh(0.2)} \quad (4)$$

where k_{ini} = initial stiffness, $\eta = 3$, $K^* = K\sqrt{(50/\sigma'_v)}$, σ'_v = vertical effective stress, and K is defined as a function φ.

2.2.4 Lim dan Jeong (2018)

The adjustment parameters for the A curve were determined to be 1,414.8 for the relative densities of Dr 80% based on

Table 1: N_{60} and V_s values derived from SPT data.

Parameters	Methods	Unit	Values				
Soil classification			**MH**	**MH**	**SC–SM**	**SC–SM**	**CL**
Depth		m	0.00–5.50	5.50–8.50	8.50–11.50	11.50–14.50	14.50–17.50
$\bar{N}_{60}$			12	11	14	28	34
V_s	Maheswari et al. [13]	m/s	176.67	172.18	194.68	233.75	243.14
	Hasancebi and Ulusuay in Hammam and Eliwa [12]		204.80	200.34	208.53	249.35	269.12
	Tsiambaos and Sabatakakis [14]		237.39	230.90	209.41	269.15	334.70
Parameters	**Methods**	**Unit**	**Values**				
Soil classification			**MH**	**SM**	**SM**	**MH**	**CL–ML**
Depth		m	17.50–20.00	20.00–23.50	23.50–26.50	26.50–29.50	29.50–30.00
$\bar{N}_{60}$			44	68	55	54	55
V_s	Maheswari et al. [13]	m/s	263.66	296.06	279.39	279.36	241.78
	Hasancebi and Ulusuay in Hammam and Eliwa [12]		288.43	314.14	296.83	303.06	305.09
	Tsiambaos and Sabatakakis [14]		365.18	372.23	343.76	388.62	456.36

Note: MH = Elastic silt ; SC–SM = Silty, clayey sand ; CL = Lean clay ; SM = Silty sand; CL–ML = Sandy silty clay ;

the linear regression analysis. Based on these results, the empirical equation for K can be calculated as follows [11]:

$$K = AP_a \left(\frac{\sigma'_v}{P_{atm}}\right)^{0.5} \quad (5)$$

$$= 1{,}414.8\ P_a \left(\frac{\sigma'_v}{P_{atm}}\right)^{0.5}, \text{for dense sand } (D_r\ 80\%) \quad (6)$$

where A = empirical depth correction coefficient, σ'_v = vertical effective stress, and P_{atm} = atmospheric pressure.

3 Methodology

Lateral pile analysis was analyzed by a numerical method based on 2D and 3D finite elements. The load-deflection analysis (p–y curve) was calculated by comparing the results of the previous research by Klinkvort (2012), Liang et al. (2018) [10], and Hyunsung and Sangseom (2018) [11] for cohesionless soil. The computer program's lateral load input is the load combination lateral loads value.

This study also examines their behaviors at various combination lateral loads (P), pile stiffness (E_p), and soil stiffnes (E_s). The combination lateral loads consist of lateral earth pressure on semi-basement walls, and the earthquake load by static equivalent method was taken based on the value of the Risk-Targeted Maximum Considered Earthquake (MCE_R) acceleration spectral response parameter mapped for a short period (S_s) and 1.0 s period (S_1): S_s = 0.80 and S_1 = 0.40, S_s = 1.00 and S_1 = 0.40, and S_s = 1.20 and S_1 = 0.50. Soil stiffness was compared using the value of shear wave velocity (V_s) derived from SPT data (Table 1) values using methods from Hasancebi and Ulusuay (2006) in Hammam and Eliwa (2013) [12], Maheswari et al. (2010) [13], and Tsiambaos and Shabatakakis (2011) [14], while the pile stiffness appealed to the value of concrete quality of K-250, K-350, and K-450.

3.1 Site Characteristics

The substructure is a reinforced concrete bored pile. Soil evaluation was conducted by the Laboratory of Soil Mechanics and Geology, Faculty of Engineering, Brawijaya University, from two SPT (Standard Penetration Test) and four CPT (Cone Penetration Test) of 2.5 tons. The study location is presented in Figure 3 around the DB. 1 drill (Figure 3).

The bored pile elevation starts at 4.325 m below the ground level (Figure 4). The bored pile elevation at 4.325 m below the ground level is assumed to be 0.00 m in modeling for finite element software. SPT elevation is 6.00

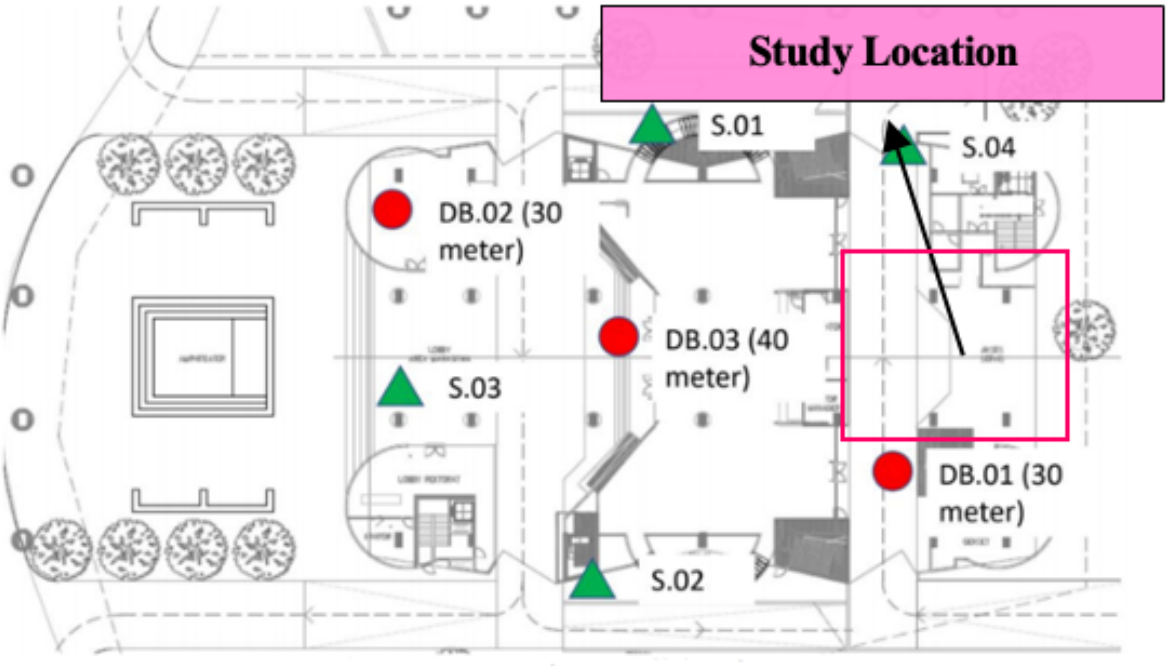

Figure 3: Site of the study.

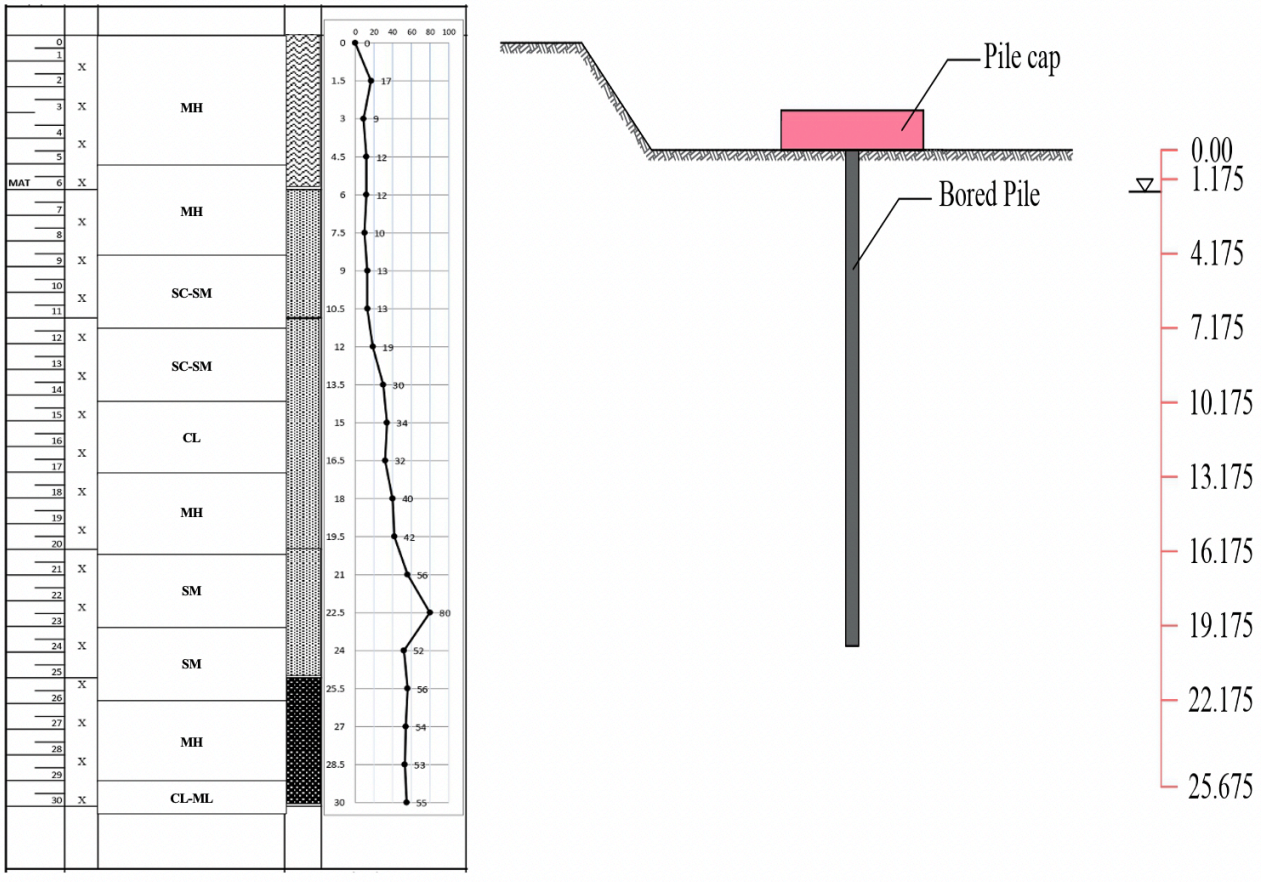

Figure 4: Bore pile elevation.

Table 2: Modulus of elasticity.

Parameters	Symbol	Unit	Values				
Soil classification			**MH**	**MH**	**SC–SM**	**SC–SM**	**CL**
Depth		m	0.00–5.50	5.50–8.50	8.50–11.50	11.50–14.50	14.50–17.50
Shear modulus	G_{max1}	kN/m²	31,512.89	30,168.81	54,463.84	58,647.40	62,843.00
	G_{max2}	kN/m²	42,346.40	40,843.44	62,487.42	66,734.39	76,989.80
	G_{max3}	kN/m²	56,897.20	54,258.68	63,015.42	77,752.24	119,082.54
Modulus of elasticity	E_{s1}	kN/m²	80,257.83	76,107.67	141,750.84	157,208.03	172,158.08
	E_{s2}	kN/m²	107,848.87	103,036.85	162,633.48	178,885.72	210,913.15
	E_{s3}	kN/m²	144,907.24	136,879.86	164,007.69	208,419.75	326,226.01
Parameters	**Symbol**	**Unit**	**Values**				
Soil classification			**MH**	**SM**	**SM**	**MH**	**CL–ML**
Depth		m	17.50–20.00	20.00–23.50	23.50–26.50	26.50–29.50	29.50–30.00
Shear modulus	G_{max1}	kN/m²	71,347.32	137,818.78	132,539.58	81,007.64	66,740.49
	G_{max2}	kN/m²	85,382.60	155,159.96	149,607.27	95,333.66	106,266.07
	G_{max3}	kN/m²	136,865.04	217,852.44	200,658.77	156,762.39	237,768.36
Modulus of elasticity	E_{s1}	kN/m²	199,772.48	385,892.57	371,110.81	226,821.40	186,873.38
	E_{s2}	kN/m²	239,071.29	434,447.88	418,900.34	266,934.24	297,544.98
	E_{s3}	kN/m²	383,222.10	609,986.82	561,844.55	438,934.70	665,751.40

m below the ground surface and is assumed at a depth of –1.675 m in the case of groundwater level.

3.2 Loads and Material Characteristics

The main function of the structure is as an educational facility and has a hazard category IV. The combination of lateral loads consists of equivalent static earthquake loads and live loads in the semi-basement based on Standard National Indonesia (SNI) 1726 [15]. Lateral earth pressure was calculated using the Coulomb method based on Das [16]. The loading consists of three conditions based on the acceleration spectral response parameter for a short period (S_s) and for 1.0-s period (S_1), including the first condition with S_s = 0.80, S_1 = 0.30, condition 2 with S_s = 0.90, S_1 = 0.40, and condition 3 with S_s = 1.00, S_1 = 0.50. The combination lateral load value of the single pile load is 542.453 kN for the first condition, 690.240 kN for the second condition, and 822.309 kN for the third condition.

Poulos & Davis [17] proposed a method for classifying piles into different categories based on the flexibility factor, Kr (Kr = $E_p I_p / E_s L_p 4$), where I_p is the inertia moment of pile and L_p is the pile length. The classification of the bored pile at Brawijaya University consists of a flexibility factor of 44 ´ 10^{-5} from E_{p1} = 20.75 MPa, 52 ´ 10^{-5} from E_{p2} = 29.05 MPa, and 59 ´ 10^{-5} from E_{p3} = 37.35 MPa. From this value, based on Li et al. [18], the piles are categorized as very flexible piles with a flexibility factor of 10^{-5}.

Based on the SPT and V_s values calculated using the approach of Hasancebi and Ulusuay in Hammam and Eliwa [12], Maheswari et al. [13], and Tsiambaos and Shabatakakis [14], the site classification is in the medium soil category (SD) based on SNI 1726 [15]. Moreover, the values of N and V_s are 15–50 and 175–350, respectively. The value of the shear wave velocity is used to determine the value of G_{max} (Table 2). In the finite element analysis, the pile is modeled linear elastic. The failure criteria are evaluated based on Mohr–Coulomb's strength parameters (friction angle) and c (cohesion).

3.3 Finite Element Method

A single pile is modeled with the material embedded beam rows (Figure 5a) for 2D analysis in PLAXIS 2D and a volume pile for 3D analysis in PLAXIS 3D (Figure 5b). The embedded beam row feature creates new possibilities for element modeling with soil–structure interactions. Embedded beam row has several advantages of plate and node to anchor nodes. It has a similar plate and meshes elements to node anchorage [19]. For software input, in the

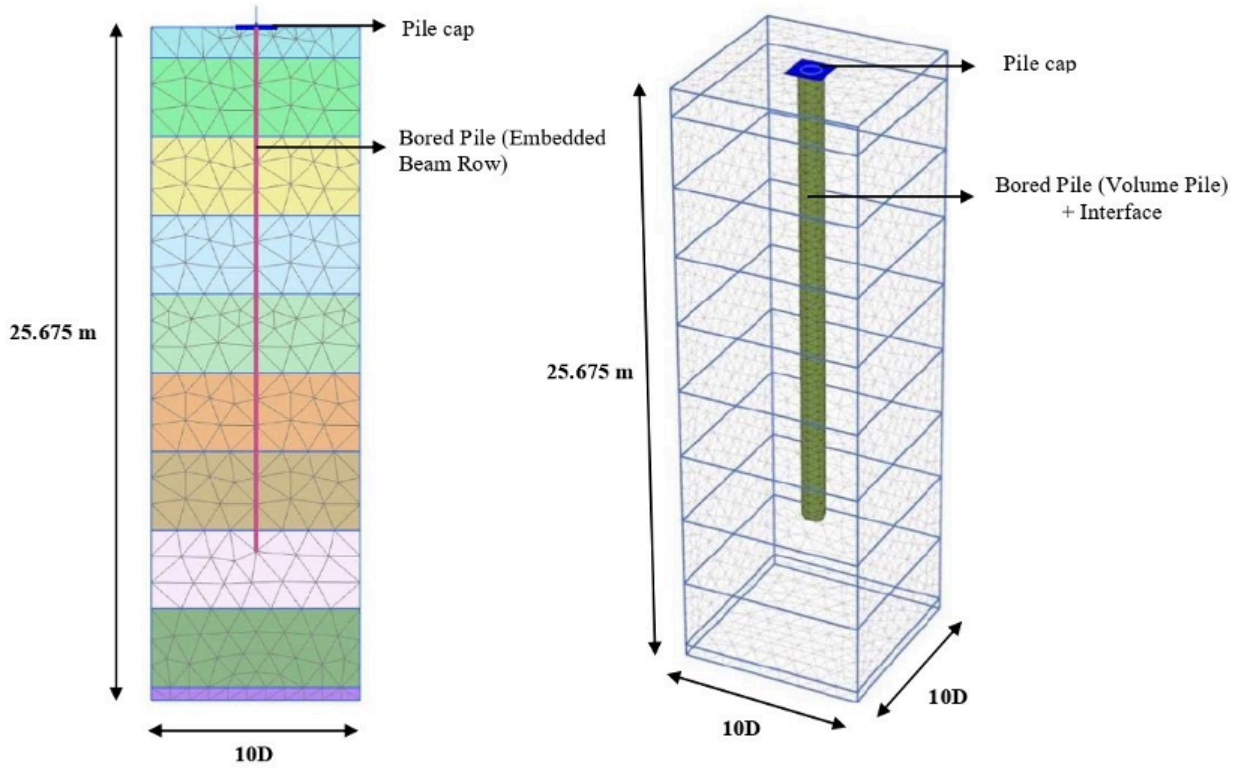

Figure 5: Pile modeling: (a) 2D finite element (b) 3D finite element.

case of static equivalent load, the axial and lateral loads are point loads with a load value equal to the allowable axial bearing capacity and three conditions of combination lateral loads. The allowable axial bearing capacity value is 956.495 kN, that calculated by the laboratory method from FHWA-NHI-10-016 [20] for cohesive soils and Yu et al. [21] for cohesionless soil. The values of x-max, x-min, y-max, and y-min are obtained as 5D from the global coordinator. The x-max and y-max value is 4 m, and the x-min and y-min value is –4 m. The modeled pile is 20 m long.

The pile interface is represented by spring at numerical stiffness in the axial and lateral directions for 2D analysis [19]. In the 3D finite element (Figure 5b), the interface presents the interaction between the structural element and the soil with a value below 1.0 to indicate friction between the structural element and the soil [22]. The mesh is a triangular element 15-node for 2D analysis and is tetrahedral 10-node for 3D analysis. The mesh becomes denser the closer it is to the pile [4]. This is different in 2D finite element analysis with embedded beam rows, where the mesh has the same size, while in 3D finite element analysis, it is appropriate that the mesh is getting denser as it gets closer to the pile structure.

4 Results and Discussion

4.1 Single Pile Lateral Load Capacity

Finite element analysis shows the flexible pile features [6]. According to this study, it is in the very flexible pile category. This is also the mechanism of pile failure in this study, characterized by pile buckled to the right from a depth of 0.00–6.00 m for 2D finite element analysis and 0.00–4.00 m for 3D finite element analysis (Figure 6a, b). Small-diameter piles show a passive wedge collapse up to 5D at shallow depth, with deflection decreasing to zero at more than 8D below the surface (Wang et al., 2020). If gaps in the soil–pile interface occur, pile stiffness can impact the depth of the gap. This is because the depth of gap expansion must be limited to the depth of the point of rotation. Below the point of rotation and on the back side of the direction of loading, the pile shifts concerning the ground. Due to suction, the transition depth from wedge failure to flow around the failure is potentially reduced for flexible piles [23]. In addition, the mechanism of the pile collapse can also be clarified by the direction of the vector which points to the right, namely, the direction of the pile fracture (Figure 6c, d).

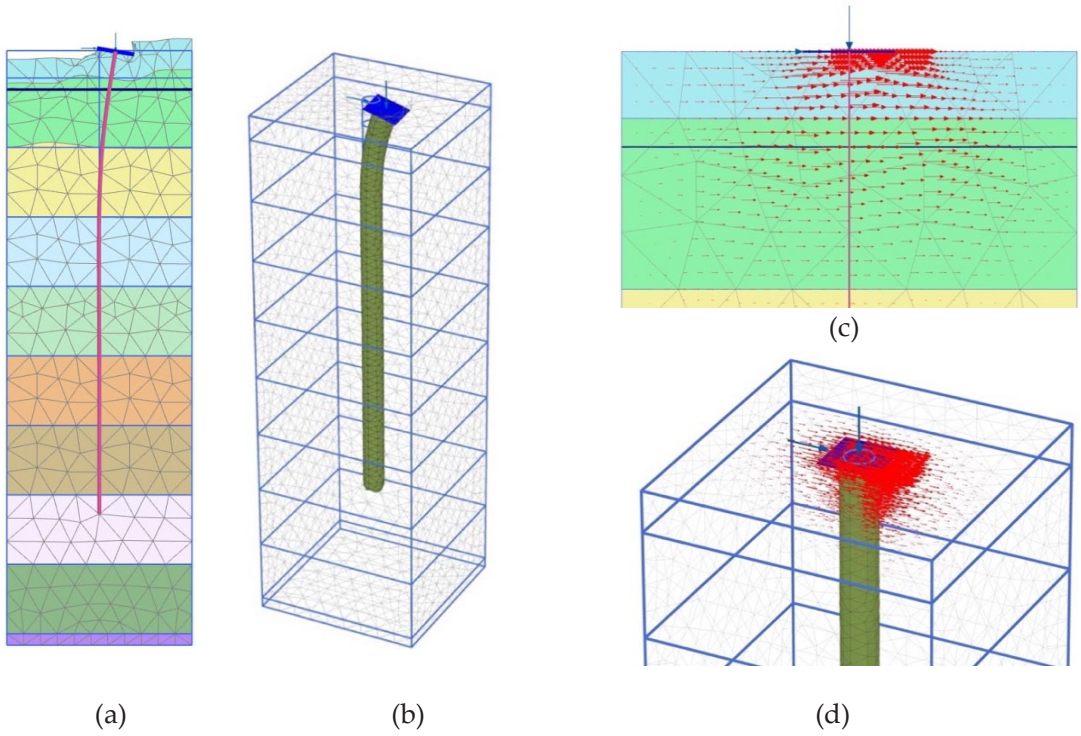

Figure 6: (a) Failure mechanism of 2D single pile. (b) failure mechanism of 3D single pile. (c) vector direction of 2D single pile. (d) vector direction of 3D single pile.

Lateral mobilization of the soil by the pile is calculated from the distribution of shear forces on the embedded beam row and volume pile. Then, it is assessed whether the lateral capacity of the soil is exceeded. Figure 7 shows a graph of the lateral load that the pile can withstand and the value of the deflection. If the pile is given a load of 542.453 kN for condition 1, 690.240 kN for condition 2, and 822.309 kN for condition 3, the combination of lateral loads' effect, pile stiffness, and soil stiffness effect on a single pile 3D analysis can withstand a load of 300 kN lower than the given load under these three conditions. 2D analysis can withstand a 400–600 kN load lower than the given load under these three conditions. The value of the lateral capacity above is within safe limits because the ultimate lateral bearing capacity of the pile (P_{ult}) happens at a load of 1,000 kN.

In 2D finite element analysis, as the combination of lateral loads increases (Figure 7a), the lateral loads increase, followed by increasing deflections. In contrast to the effects of pile stiffness (Figure 7b) and soil stiffness (Figure 7c), the pile stiffness increases, deflection decreases, and lateral loads decrease. Regarding the effect of soil stiffness, where the soil stiffness increases, the deflection decreases, but the lateral load increases. This is in agreement with the results of [24], which states that when E_s increases, the deflection does not increase significantly.

As is the case in 3D finite element analysis, when the combined lateral load increases, the deflection increases and the lateral load increases. Regarding the effect of pile stiffness, with increasing flexural stiffness, the pile behavior is still governed by the wedge failure mechanism [6]. In addition, as the pile stiffness increases, the deflection decreases, but the lateral load increases, contrary to the results proposed by Wang et al. [6] that stiffer pile deflection under the same lateral load is slightly underestimated and due to the more considerable flexural stiffness, for the same deflection at ground level, a larger soil zone is mobilized. The depth of the effect of wedge failure also increases. With regard to the effect of soil stiffness, where the stiffness of the soil increases, the deflection decreases, followed by a decrease in the lateral load. According to the study by Zhou et al. [24], the displacement of the tip of the pile decreases with increasing E_s. It can be seen that 2D has different behavior from 3D finite element analysis on the effects of pile stiffness and soil stiffness. The 3D numerical model is reliable for improving the soil–pile reaction while decreasing the overall flexural stiffness of the pile friction [25]. The 3D finite element analysis is related to the soil response [26],

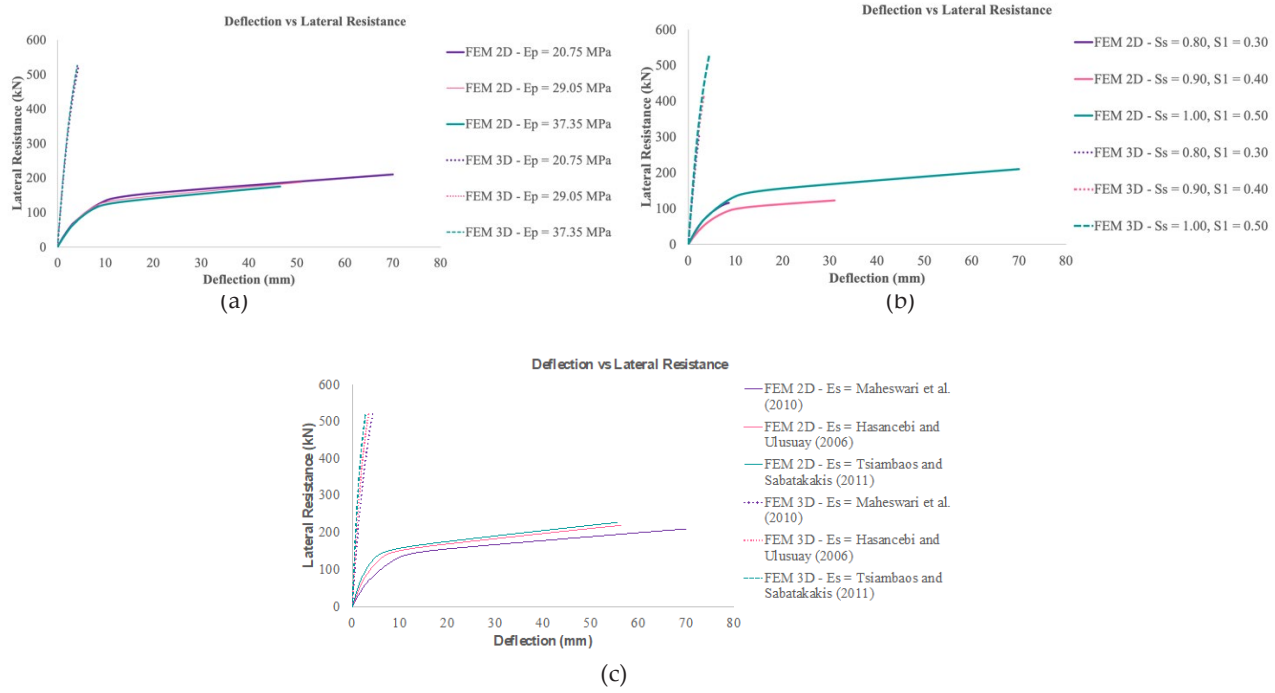

Figure 7: Lateral load capacity versus deflection: (a) combination lateral loads effect, (b) pile stiffness effect, (c) soil stiffness effect.

Table 3: The difference in lateral resistance with the FEM 3D.

	Lateral resistance (kN)		Difference in lateral resistance with FEM 3D (%)
	FEM 2D	FEM 3D	
Combination lateral loads effect			
P_{S1}	115.808	304.663	61.988
P_{S2}	118.323	414.567	71.459
P_{S3}	210.442	524.270	59.860
Pile stiffness effect			
E_{p1}	210.442	524.270	59.860
E_{p2}	187.449	525.274	64.314
E_{p3}	175.958	526.043	66.551
Soil stiffness effect			
E_{s1}	210.442	524.270	59.860
E_{s2}	219.603	522.476	57.969
E_{s3}	227.736	520.390	56.237

as evidenced by the deflection occurring less than 25 mm, by the permissible deflection for the lateral pile based on Isenhower et al. [7], while the 2D analysis has a deflection more significant than 25 mm (Figure 7).

Furthermore, the 3D finite element showed the deflection was 1%D and the 2D finite element showed the deflection was 4%–8%D. The lateral load-deflection curves calculated from the 3D finite element analysis correspond to the validation for lateral load–soil interaction [27]. It can be seen that the deflection of the 2D finite element analysis on the effect of soil stiffness is inversely related to the lateral load, and the deflection of the 3D finite element analysis on the effect of pile stiffness is also inversely related to the lateral load.

The average difference in the lateral resistance of the 2D single pile analysis compared to the 3D single pile analysis was 50%–70% (Table 3) and the deflection was 70%–90% (Table 4). It can be seen that the difference between 2D and 3D analyses is vast, where 2D finite element analysis reduces the lateral resistance but increases the deflection at the pile surface. Considering that the friction factor is related to the strength properties of the soil layer, this is because there is no friction factor or interface in the embedded beam row model. The interface is represented by a spring. The spring is most likely to cause a decrease in stiffness and friction between the soil and piles. Thus, the deflection is large and the strength of the soil layer decreases due to the interaction between the piles in contact. So, they do not slip over each other. This is different from Sluis et al. [1] which reports that the shear force of structural elements in the 2D model will be

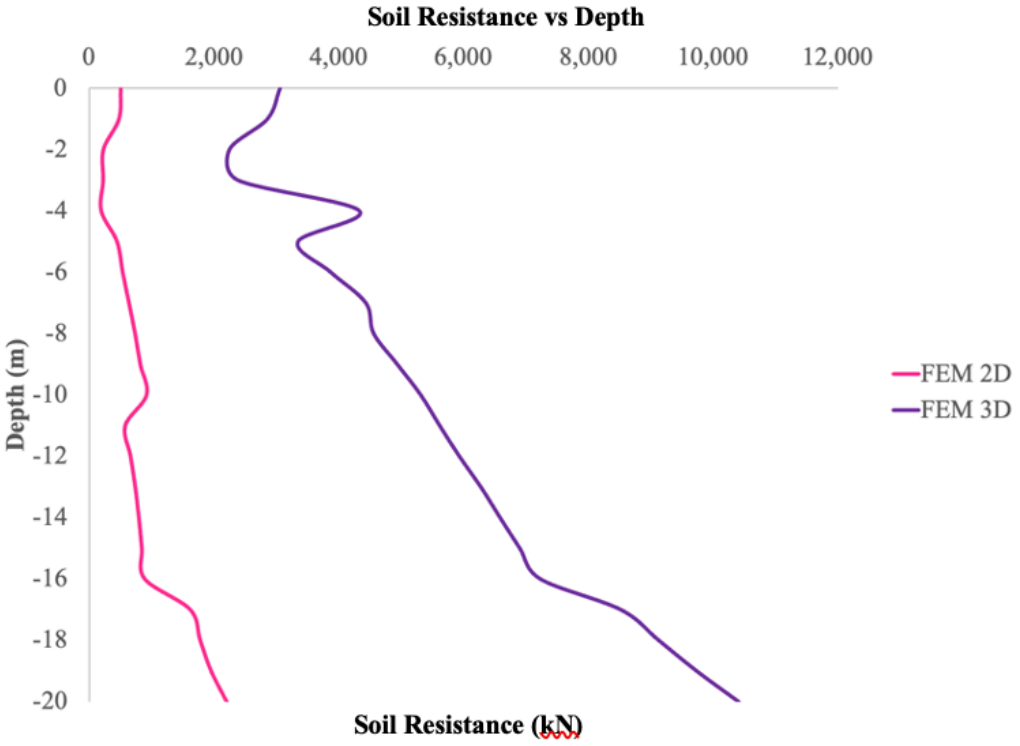

Figure 8: Lateral bearing capacity.

Table 4: The difference in deflection with the FEM 3D.

	Deflection (mm)		The difference in deflection with FEM 3D (%)
	FEM 2D	FEM 3D	
Combination lateral loads effect			
P_{S1}	8.646	2.417	72.044
P_{S2}	31.044	3.532	88.622
P_{S3}	70.132	4.972	92.911
Pile stiffness effect			
E_{p1}	70.132	4.972	92.911
E_{p2}	50.969	4.808	90.567
E_{p3}	46.492	4.692	89.909
Soil stiffness effect			
E_{s1}	70.132	4.972	92.911
E_{s2}	56.430	3.939	93.020
E_{s3}	55.688	3.140	94.362

greater than in the 3D model. Based on these results, the behavior of the lateral pile using 2D finite element analysis is considered inconsistent.

In addition, 3D finite element analysis has a friction factor (interface), which can increase the interaction between the pile and soil by slipping the two materials against each other. This makes the 3D numerical model appropriate to be relied upon to improve the pile–soil reaction.

4.2 Soil Lateral Bearing Capacity

The mobilization of the lateral bearing capacity of the soil by the pile is calculated based on the equivalent force of the soil stress that occurs in the x direction. This assessment is carried out per unit meter depth over the total pile length (Figure 8). Combination lateral loads effect, pile stiffness effect, and soil stiffness effect do not affect the soil's lateral bearing capacity because the soil's lateral bearing capacity is based on soil characteristics such as soil unit weight and friction angle. The ultimate lateral bearing capacity, p_u, increases with increasing depth [6,27]. The ultimate lateral bearing capacity has the largest value based on the 3D finite element method. The lateral bearing capacity of the soil is fully mobilized along the full depth of the pile, lowering the ultimate resistance of the soil at shallow depths and increasing it in the deep zone. This agrees with [6,9,27] that the ultimate lateral bearing capacity, p_u, increases with increasing depth.

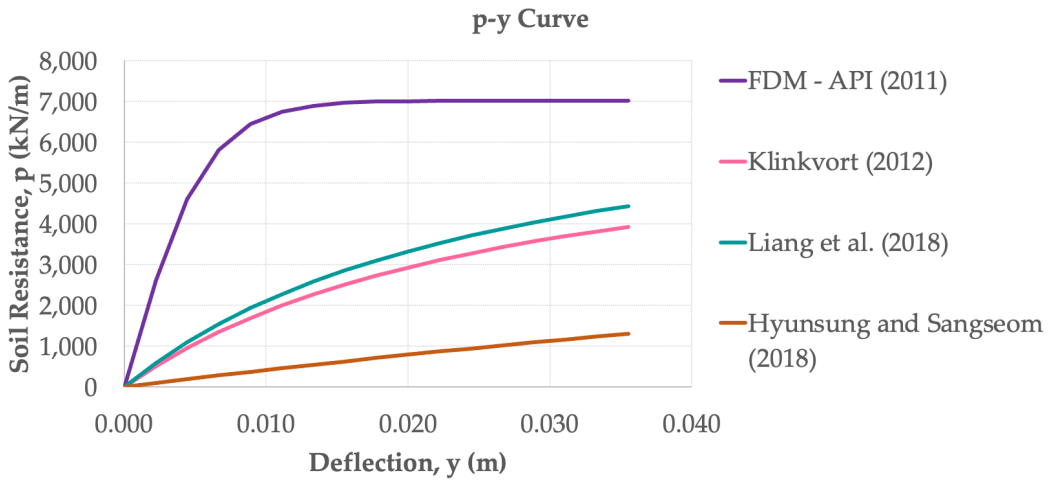

Figure 9: p–y curve.

Table 5: The difference in deflection with the FEM 3D.

	Lateral resistance (kN)	The difference in deflection with FEM 3D (%)	The difference in deflection with FEM 2D (%)
FEM 3D	10,410.00	-	81.220
FEM 2D	1,955.00	81.220	-
FDM – API (2011)	7,025.381	32.513	72.172
Klinkvort (2012)	3,931.621	62.232	50.275
Liang et al. (2018) [10]	4,441.177	57.337	55.980
Hyunsung and Sangseom (2018) [11[	1,306.272	87.452	33.183

4.2.1 The p–y Curve

The p–y curve was obtained with the help of finite difference software for a single pile calculated using the p–y API approach [9]. Pile modeling at the finite difference method is identical to the 3D finite element method, and the relationship between soil resistance and deflection (p–y curve) was taken at a depth of 20.00 m to match the pile group's deflection output from the 3D finite element analysis. The FDM – API method has the highest lateral soil resistance value, followed by the method of Klinkvort (2012), Liang et al. (2018) [10] in the second place, and Hyunsung and Sangseom (2018) [11] are the lowest. In contrast to a study by Wang et al. [27], the Klinkvort method increases k_{ini} at greater depths. The Klinkvort method has lower soil lateral resistance values [6,27]. The three methods continue to increase until it reaches the maximum lateral soil resistance at maximum deflection (Figure 9). Meanwhile, it increases until it reaches the maximum lateral soil resistance at a deflection of 0.125%D and then becomes constant until the maximum deflection is achieved.

The load–displacement relationship calculated by the FDM – API presents a good agreement with the 3D finite element analysis with a difference of 30% (Table 5). The 3D finite element analysis increases soil stiffness at greater depths. It is appropriate that the API method estimates the lateral pile–soil resistance due to the API method [9], inducing an overestimation of the initial stiffness, and the API method [9] provides reasonable predictions for small-diameter piles [6,27]. The FDM – API method significantly overestimates the present value at all depths (Figure 9). Moreover, the API method [9] is defined as a cyclic p–y curve related to small-diameter flexible piles, and therefore, it overestimates the soil reaction at higher depths. The increase in soil reaction might be due to an additional component of the soil reaction by pile rotation to the simple lateral translational mode of pile deformation [5,6]. The p–y curve is more rigid than the other methods, considering the initial stiffness and the final lateral stress [28]. In addition, the load–displacement relationship calculated by Hyunsung and Sangseom [11] agrees well with the 2D finite element (Table 5). In contrast to 3D finite element analysis, in 2D finite element analysis,

it is possible to reduce stiffness because there is no friction between the soil and piles.

5 Conclusion

With the increase of the earthquake intensity in Indonesia, especially in Malang, East Java, it is still rare to compare the pile model with embedded beam row for 2D analysis, and volume pile in the 3D analysis is still rarely done, where some studies only present the results of research by modeling using one of these models without further comparing the two. This research was carried out to determine the response of a single pile, that is, the lateral resistance of pile and soil, to earthquake loads with 2D and 3d modeling. Conclusions based on the above analysis can be drawn as follows:

1. The 2D finite element analysis with embedded beam row modeling has a different behavior from 3D finite element analysis with volume pile modeling for the case of soil stiffness and pile stiffness.
2. 2D finite element analysis is considered to have inconsistent behavior, which reduces lateral resistance by a difference when compared to 3D single pile analysis was 50%–70%. In addition, the 2D finite element overestimated the deflection on the pile surface with the difference was 70%–90%. This is because in the 2D finite element modeling with an embedded beam row, the friction factor is represented by the spring, which reduces the stiffness and the pile–soil is tangent, so that there is no slipping against each other.
3. 3D finite element analysis can improve the interaction between the soil and pile because it has a friction factor (interface); so, the deflection that occurs is less than the allowable deflection.
4. The load–displacement relationship calculated by the FDM – API presents a good agreement with the 3D finite element because both methods increase soil stiffness at greater depths, and the load–displacement relationship calculated by Hyunsung and Sangseom [11] presents a good agreement with the 2D finite element.

6 Suggestion

A 3D numerical model can be help improve pile–soil reaction. Lateral pile analysis can be conducted with other indicators of different effects, such as variations in the effects of axial loads and mesh effects on finite element analysis.

Acknowledgment: This study was supported by the Department of Facilities and Infrastructure, Brawijaya University, which has assisted in providing data and soil laboratories.

References

[1] Sluis, J.; Besseling F.; StuurwoldP.H.H.; *Modelling of a pile row in a 2D plane strain FE-analysis*. *Num. Method. Geotech. Eng*. **2014**, 978-1-138-00146-6.
[2] Brown, D.A.; Morrison, C.; Reese, L.C. Lateral Load Behavior of Pile Group in Sand. *J. Geotech. Eng. Am. Soc. Civil Eng*. **1988**, Volume 114, pp. 1261–1276.
[3] Hemel M.J.; Korff Mandy.; Peters D.J.; Analytical model for laterally loaded pile groups in layered sloping soil. *Marine. Struc.* **2022**, 84, 103229.
[4] Cao, G.; Ding, X.; Yin, Z.; Zhou, H.; Zhou, P. A New Soil Reaction Model for Large-Diameter Monopiles in Clay. *Comput. Geotech.* **2021**, *137*, 104311. https://doi.org/10.1016/j.compgeo.2021.104311.
[5] API. *Petroleum and Natural Gas. Industries-Specific Requirements for Offshore Structures: Part 4-Geotechnical and Foundation Design Considerations ISO 19901–4:2003*; American Petroleum Institute: Washington, DC., USA, 2014.
[6] Wang, H.; Wang, L. Z.; Hong, Y.; He, B.; Zhu, R. H. Quantifying the influence of pile diameter on the load transfer curves of laterally loaded monopile in sand. *App. Ocean. Res*. **2020**, *101*, 102196.
[7] Isenhower, W. M.; Shin-Tower, W.; Gonzalo, V. L. (2016). *Technical Manual for LPile 2016 (Using Data Format Version 9)*. Ensoft, Inc.
[8] Reese, L. C. Behavior of Piles and Pile Groups Under Lateral Load. Federal Highway Administration Office of Engineering & Highway Operations Research and Development: Washington D.C, US, 1986.
[9] API. *Petroleum and Natural Gas. Industries-Specific Requirements for Offshore Structures: Part 4-Geotechnical and Foundation Design Considerations ISO 19901–4:2003*; American Petroleum Institute: Washington, DC., USA, 2011.
[10] Liang, F.; Chen, H.; Jia, Y. Quasi-static p-y hysteresis loop for cyclic lateral response of pile foundations in offshore platforms. *Ocean. Eng.*, **2018**, *148*, 62-74.
[11] Hyunsung L.; Sangseom J. Simplified p-y curves under dynamic loading in dry sand. *Soil. Dyn. Earth. Eng*. **2018**, 113, 101–111.
[12] Hammam, A.H.; Eliwa, M. Comparison Between Results of Dynamic & Static Moduli of Soil Determined by Different Methods. *HBRC J*. **2013**, *9*, 144–149.
[13] Maheswari, R.U.; Boominathan, A.; Dodagoudar, G.R. Use of Surface Waves in Statistical Correlations of Shear Wave Velocity and Penetration Resistance of Chennai Soils. *Geotech. Geo. Eng.* **2010**, *28*, 119–137.

[14] Tsiambaos, G.; Sabatakakis, N. Empirical Estimation of Shear Wave Velocity from in Situ Tests on Soil Formations in Greece. *Bull. Eng. Geo. Env.* **2011**, *70*, 291–297.
[15] Badan Standardisasi Nasional. *Perencanaan Ketahanan Gempa Untuk Gedung dan Non Gedung [SNI 1726:2019]* [Earthquake Resistance Planning for Buildings and Non-Buildings [SNI 1726:2019]]. Badan Standardisasi Nasional: Jakarta, Indonesia, 2019.
[16] Das, B.M. *Principles of Foundation Engineering*, 7th ed. Thomson: Toronto, 2011.
[17] Poulos, H.G.; Davis, E.H. *Pile Foundation Analysis and Design*; Wiley: New York, USA, 1980. Available online: https://trid.trb.org/view/164430 (accessed on 24 May 2022).
[18] Li, Z.; Kotronis, P.; Escoffier, S. Numerical Study of the 3D Failure Envelope of a Single Pile in Sand. *Com. Geotech.* **2014**, *62*, 11–26.
[19] Sluis, J. *Validation and Application of the Embedded Pile Row Feature in PLAXIS 2D*. Plaxis Bulletin: Autumn issue. 2013.
[20] FHWA-HIF-18-031. (2018). *Geoetchnical Engineering Circular: Design, Analysis, and Testing of Laterally Loaded Deep Foundations that Support Trannsportation Facilities*. U.S. Department of Transportation; Federal Highway Administration.
[21] Yu, X.; Abu-Farsakh, M. Y.; Yoon, S.; Tsai, C.; Zhang, Z. Implementation of LRFD of drilled shafts in Louisiana. *J. Infra. System.* **2012**, *18*(2), 103-112.
[22] Tjie-Liong, G. Common Mistakes on the Application of Plaxis 2D in Analyzing Excavation Problems. *Int. J. App. Eng. Res.* **2014**, *9*, 8291–8311.
[23] Zhang, Y.; Andersen, K. H.; & Tedesco, G. Ultimate bearing capacity of laterally loaded piles in clay–Some practical considerations. *Marine. Struc.* **2016**, *50*, 260-275.
[24] Zhou, P.; Zhou, H.; Liu, H.; Li, X.; Ding, X.; Wang, Z. Analysis of lateral response of Existing Single Pile Caused by Penetration of Adjacent Pile in Undrained Clay. *Comput. Geotech.* **2020**, *126*, 103736.
[25] Zhu, B.; Wen, K.; Kong, D.; Zhu, Z.; Wang, L. A Numerical Study on the Lateral Loading Behaviour of Offshore Tetrapod Piled Jacket Foundations in Clay. *App. Ocean. Res*. **2018**, *75*, 165–177.
[26] Youngho, K.; Sangseom J. Determination of depth-of-fixity point for laterally loaded vertical offshore piles: A new approach. *Comput. and Goetech.* **2011**, 38, 248–257.
[27] Wang, H.; Wang, L.; Hong, Y.; Mašín, D.; Li, W.; He, B.; Pan, H. Centrifuge testing on monotonic and cyclic lateral behavior of large-diameter slender piles in sand. *Ocean. Eng.* **2021**, *226*, 108299.
[28] Zhang H.; Liu R.;, Yuan Y. Influence of spudcan-pile interaction on laterally loaded piles. *Ocean. Eng*. **2019**, 184, 32–39.